ASTRONOMY
AND
ASTROPHYSICS

Constraints on the abundances of various molecules in interstellar ice: laboratory studies and astrophysical implications

Nathalie Boudin[1,2]**, Willem A. Schutte**[1]**, and J. Mayo Greenberg**[1]

[1] Leiden Observatory, P.O. Box 9513, 2300 RA Leiden, The Netherlands
[2] Ecole Nationale Supérieure de Chimie et de Physique de Bordeaux, Avenue Pey Berland, B.P. 108, F-33402 Talence Cedex, France

Abstract. Ethane, acetylene, ethanol, hydrazine and hydrogen peroxyde are either predicted by theoretical models to be abundant in the icy mantles on grains in dense clouds, or were found to be produced by comets. We present measurements of the spectra of these species embedded in astrophysically relevant ice matrices. Additionally, we obtained the spectrum of the hydrozonium ion ($N_2H_5^+$) which could be produced by activation-less acid-base reactions. The laboratory results are compared to the ISO and ground–based spectra of NGC 7538:IRS 9. Strict upper-limits compared to the solid water could be found for ethane, ethanol and hydrogen peroxyde of $< 0.4\%$, $< 1.2\%$, and $< 6.1\%$, respectively. These results give some important information on the relationship between cometary and interstellar ices and on the nature of grain surface reactions.

Key words: methods: laboratory – stars: individual: NGC 7538:IRS 9 – ISM: molecules – ISM: abundances – infrared: ISM: lines and bands

1. Introduction

It is generally thought that the ices in interstellar clouds form when molecules collide with and stick on dust particles. Before being incorporated in the icy mantles, grain surface reactions can reduce or oxidize reactive species. Models of gas phase and grain surface- or photo-chemistry can reasonably reproduce the observed composition of the ices, which consist of H_2O (the dominant component), CO, CO_2, CH_3OH, CH_4 and some trace constituents (Tielens & Hagen 1982, d'Hendecourt et al. 1985, Hasegawa et al. 1992, Hasegawa & Herbst 1993, Shalabiea & Greenberg 1994; Schutte 1996, Whittet et al. 1996). However, subsequent experimental results indicate that the efficiency of both photochemical and surface chemical pathways (i.e., surface hydrogenation of CO) for the production of CH_3OH are

Send offprint requests to: W.A. Schutte

strongly overestimated by the models (Schutte et al. 1996a, Hiraoka et al. 1994). Thus, considerable uncertainty remains on the formation mechanism for this molecule, which generally is found in interstellar ices at an considerable abundance.

Models also predict that a number of other species could have appreciable abundances in the icy mantles ($\lesssim 1\%$), e.g., the relatively large molecules C_2H_6 and CH_3CH_2OH (Hasegawa & Herbst 1993, Charnley et al. 1995). Moreover, a number of molecules are present in comets which have not yet been found in interstellar ice, for example C_2H_2 and C_2H_6 (Mumma et al. 1996, Bockelée-Morvan 1997). Constraining the abundances of such species in interstellar ice could thus inform us about the nature of the chemical processes which were involved in the formation and further evolution of the ices. Also, it could provide insight into the relation between interstellar ice and comets.

In this paper we report an infrared spectroscopic study of six species which are predicted to be important constituents of interstellar ice and/or which have been observed in comets. These are ethane (C_2H_6), acetylene (C_2H_2), ethanol (CH_3CH_2OH), hydrazine (N_2H_4), hydrogen peroxyde (H_2O_2) and the hydrozonium ion ($N_2H_5^+$). The spectra of the species were measured in astrophysically relevant ice matrices, i.e., water-dominated ice and CO-dominated ice, as well as for pure ice samples of the various species. These results can be used to search for their infrared signature towards sources obscured by dense cloud dust.

Gas-phase ion-molecule reactions cannot produce ethane at low temperatures because most of the relevant reactions are endothermic (Herbst et al. 1983). But ethane can be created efficiently via grain surface reactions involving hydrogenation of atomic carbon, the C_2 radical, acetylene condensed from the gas phase and light radicals consisting of C and H (Prasad et al. 1987, Hasegawa et al. 1992). When allowing tunnelling reactions, hydrogenation via H_2 enhances the production efficiency of ethane, as well as methane (Hasegawa & Herbst 1993). Additionally, UV photolysis of CH_4-rich ice may contribute to the production of ethane (Gerakines et al. 1996). Starting with a largely atomic gas, the abundance of ethane in the icy mantles

was calculated as 0.2% to 0.5% (Hasegawa & Herbst 1993). Its homologue, methane is, in this case, about three times as abundant. Recently, ethane was detected in Comet C/1996 B2 Hyakutake at an abundance relative to H_2O of 0.4%, close to the 0.7% abundance for methane (Mumma et al. 1996). The prediction by thermochemistry if one assumes that the origin of this comet is in the equilibrated region of the solar nebula gives orders of magnitude smaller ethane-methane ratio. This ratio may thus be explained by kinetically controlled formation on grains in the interstellar dense cloud core that preceded the solar system, consistent with comets having formed from material of the pre-solar molecular cloud with little alteration (Greenberg 1982). A search for ethane in interstellar ices provides an important test of this hypothesis: the ratio of ethane and methane abundances must be comparable to that of Hyakutake for protostellar regions which are comparable to the pre-solar nebula.

Acetylene can be formed in the gas-phase by ion-molecule chemistry (Prasad et al. 1987). However, its gas-phase abundance is strongly enhanced in warm cloud regions, implying its injection from subliming icy grain mantles (Brown et al. 1988, Lacy et al. 1989, Carr et al. 1995, Evans et al. 1991). For example, the model of Brown et al. (1988), in which acetylene is formed in the gas phase, collected on the icy grain mantles during a cold cloud phase and subsequently evaporates upon protostar formation, is able to reproduce the high gas phase acetylene abundance in the Orion IR cluster (Evans et al. 1991). In this model, the amount of solid acetylene can be as high as 0.5% relative to H_2O. More sophisticated models (Hasegawa & Herbst 1993) take into account grain surface reactions. In these models, acetylene can be destroyed by grain surface hydrogenation producing ethane. While the surface reactions may produce some acetylene as well, the net result is a decrease of the acetylene abundance in the icy mantles. However, since the predicted acetylene abundance is too low to explain the large quantities observed towards the IR cluster (Evans et al. 1991), perhaps the hydrogenation of acetylene is somewhat less efficient than assumed in these models. An acetylene abundance of 0.3% to 0.9% has been reported for Comet C/Hyakutake (Bockelée-Morvan 1997).

In dense cores, where star formation occurs, ethanol is observed at an abundance which is many orders of magnitude in excess of predictions based on pure gas-phase chemistry (Millar et al. 1995). One explanation is that grains could hold an appreciable amount of ethanol ice which is released in the gasphase via sublimation (Charnley et al. 1995). From the constraints imposed by the gas-phase abundance, an initial amount of solid ethanol between 0.5% and 5% relative to H_2O is indicated. Ethanol can be created in icy grain mantles via different pathways. Tunneling reactions may allow production by the hydrogenation of acetylene (Hasegawa et al. 1992) followed by an oxidation of the produced alkyl radicals. Furthermore ethanol could be produced by radical-radical surface reactions, involving CH_2, CH_3 and OH. In contrast, its homologue methanol may, besides by radical-radical reactions, also be produced by hydrogenation of the very abundant carbon monoxide molecule

(Hasegawa & Herbst 1993, Hiraoka et al. 1994). Thus the abundance of ethanol and the methanol/ethanol ratio in interstellar ices may give important information on the nature of grain surface chemistry.

In the gas phase, nitrogen is predicted to be predominantly in the form of molecular nitrogen N_2, a very stable molecule. N_2 can freeze onto the grain mantles and by hydrogenation produce diimide (N_2H_2). It is unclear whether further hydrogenation may proceed, resulting in hydrazine, or whether hydrogen abstraction would be favored, in which case diimide would be the most hydrogenated product of molecular nitrogen (Tielens & Hagen 1982). If grain surface hydrogenation of N_2 to N_2H_4 is efficient, solid hydrazine abundances as high as 5% relative to H_2O may be possible (Hasegawa & Herbst 1993).

The existence of interstellar acids or bases can modify the classical network of the radical-radical grain surface reactions (Grim et al. 1989, Schutte & Greenberg 1997). If some energy source is available like the heat of condensation of species onto the grain, the heat produced by surface reactions or the energy carried by UV rays, acids and bases can react leading to production of ions. Hydrazine being a very strong base, this molecule could be converted to the hydrozonium ion $N_2H_5^+$ in the presence of acids like cyanic acid HOCN or formic acid HCOOH.

Hydrogen peroxide can be produced on grain surfaces via the hydrogenation of molecular oxygen. Hydrogen peroxide may subsequently be destroyed by H atoms resulting in H_2O and possibly HO_2 (Tielens & Hagen 1982, Hasegawa et al. 1992, Hasegawa & Herbst 1993). The models predict an "equilibrium" abundance up to 5 % relative to H_2O.

This paper is laid out as follows. In Sect. 2 we briefly review the experimental details. Sect. 3 presents the spectroscopic results for the six species which are the subject of this study. Sect. 4 uses these results to constrain the abundances of these species in interstellar ice. In Sect. 5 the astrophysical implications with respect to the nature of grain surface chemistry and the relationship between interstellar and comet ices are discussed. Sect. 6, finally, briefly summarizes the conclusions of this study.

2. Experimental

The general procedure for creating the ice samples and their infrared spectra has been described earlier (Gerakines et al. 1995). Compounds used in this work and their purities are as follows: C_2H_6 (gas), Praxair, 99.99% purity; C_2H_2 (gas), Praxair, 99.6% purity and CH_3CH_2OH (liquid), Merck, 99.8% purity. Hydrazine and hydrogen peroxide were in aqueous solution where the concentration of N_2H_4 (Aldrich) was 50% and of H_2O_2 (J. T. Baker) was 30%. They were purified under vacuum at 40°C while shaking. For hydrogen peroxide, the remaining water content is small but considerable water remained in hydrazine because of the small difference in the vapor pressure of these molecules. Since hydrazine slowly decomposes forming ammonia at room temperature, the purified hydrazine was stored at liquid nitrogen temperatures.

Further molecules applied in the experiments were H_2O, purified by three freeze-thaw cycles; CO (gas), Praxair, 99.997% purity and HCOOH (liquid), J. T. Baker, 98% purity.

Because of low-vapor pressure, hydrazine and hydrogen peroxide could not be pre-mixed with other gases. Mixed ices were then produced by simultaneous deposition of the subject (N_2H_4, H_2O_2) and diluting gas (H_2O, CO) through separate deposition tubes (see Gerakines et al. 1995).

3. Results

For each molecule, spectra in three ice matrices were obtained; pure, diluted in H_2O and diluted in CO. In general, the composition of the mixtures was dilutant / subject = (10–20)/1. This ratio allows for sensitive spectroscopy of the subject species, while reproducing the high degree of dilution expected for trace molecules in interstellar ices. For each molecule and matrix, the vibrational assignment, band position, full width at half maximum (FWHM), and the integrated band strength A, when available, are listed (Tables 1 to 6). In Appendix A the behaviour during warm-up of the main infrared bands of ethane, ethanol and hydrogen peroxide in the H_2O as well as CO matrices is presented.

Various ways were used to calculate integrated band strengths. In the case of a single deposition of a mixed gas consisting of the subject species (in this case ethane, acetylene and ethanol) in a diluting species (water and carbon monoxide), we used:

$$A_S(in\ D) = \frac{N_D}{N_S}\ \frac{\int_{feature}\tau_S d\nu}{\int_{feature}\tau_D d\nu}\ A_D \qquad (1)$$

where D is the dilutant and S is the subject species. The ratio of the column densities N_D/N_S is equal to the abundance ratio of the two components, known from the gas pressure in the glass vacuum manifold during mixture preparation (e.g., Boogert et al. 1997). The optical depth τ_X is measured from the spectra for both the dilutant and subject features. The integrated strengths used were A_{H_2O} (OH stretch.) = 2.0×10^{-16} cm molecule^{-1}, $A_{CO} = 1.0\times10^{-17}$ cm molecule^{-1} (d'Hendecourt & Allamandola 1986). Integrated band strengths from the literature for pure ice were used for comparison.

For the experiments involving hydrazine and hydrogen peroxide the subject and dilutant species were separately deposited. Two depositions were made, one where the subject molecule is deposited simultaneously with the dilutant (H_2O or CO) and the other with only the subject molecule. If the depositions are made for the same length of time and with the same flow rate, the deposited quantity of subject gas is equal in each deposition. The ratio of the integrated band strength of the molecule in pure ice to integrated band strength while diluted is then given by (Gerakines et al 1995):

$$\frac{A_S(in\ D)}{A_S(pure)} = \frac{\int_{feature}\tau_S(in\ D)d\nu}{\int_{feature}\tau_S(pure)d\nu}\ . \qquad (2)$$

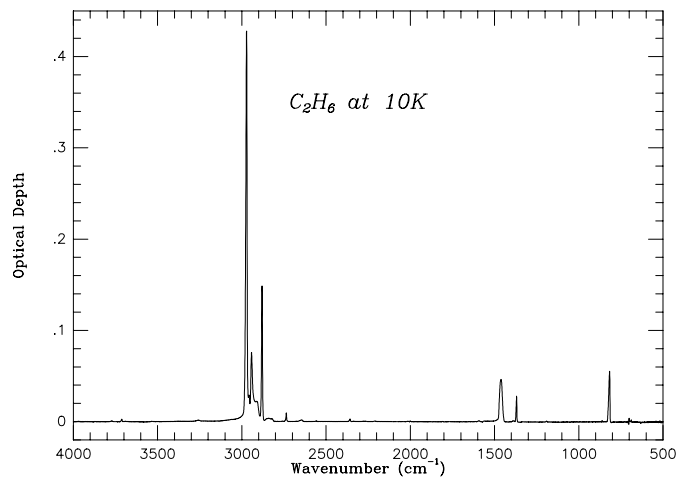The Gerakines et al. (1995) procedure was somewhat modified to meet the specific demands of these experiments. For

Fig. 1. IR spectrum of pure C_2H_6 at 10K

N_2H_4, considerable H_2O was still present after purification (N_2H_4 / H_2O = 1/3; Sect. 2). For this reason only the ratio for N_2H_4 diluted in H_2O relative to N_2H_4 diluted in CO (with some H_2O) could be obtained. The assumption was made that the integrated band strengths of the features of N_2H_4 in H_2O are equal to those of N_2H_4 pure, which was obtained from Roux & Wood (1983). In support of this assumption, it could be verified that the ratio of the strongest N_2H_4 bands, ν_{12} (1093 cm^{-1}) and ν_{11} (1345 cm^{-1}), are equal in pure ice (Roux & Wood 1983) and in H_2O / N_2H_4 = 3/1 within 5%.

For H_2O_2, only an integrated band strength in the gas phase could be found for the ν_6 (1389 cm^{-1}) feature (Valero et al. 1981). The assumption was made that the band strength is the same for H_2O_2 in the CO matrix. The H_2O_2 pure band strengths were obtained after CO sublimation upon warm-up to ~30 K. The band strength for H_2O_2 diluted in H_2O can then be obtained by the procedure outlined above.

Finally, $N_2H_5^+$ was produced by separate depositions of H_2O / N_2H_4 = 3/1 and a H_2O / HCOOH = 1/1 mixture, resulting in a H_2O / HCOOH / N_2H_4 = 20/10/3 ice. The overabundance of HCOOH, as well as warm-up to 120 K, ensured that all N_2H_4 was converted to $N_2H_5^+$, as could be verified by the disappearance of the N_2H_4 bands during the warm-up. Then, the $N_2H_5^+$ column density is equal to that of the originally deposited N_2H_4, which could be measured by seperately repeating the H_2O / N_2H_4 = 3/1 deposition (Gerakines et al. 1995).

The laboratory spectra discussed in this paper are on request available from W.A. Schutte (schutte@strwchem.strw.leidenuniv.nl).

3.1. Ethane: C_2H_6

Fig. 1 displays the IR spectrum of pure ethane ice. The strongest features are those of the CH stretching modes. Band positions with assignment, FWHM and integrated band strengths are given in Table 1. The shift of the $\nu_8 + \nu_{11}$, ν_1, ν_5, ν_{10} and ν_7 features in the three kinds of ices is shown in Fig. 2. Compared to the gas phase (Tejada & Eggers 1976), the peak positions in

Table 1. Infrared features of C_2H_6. Entries correspond to 10 K ices: pure C_2H_6; C_2H_6 / H_2O = 1/20 and C_2H_6 / CO = 1/20

Mode[a]	Position: ν (cm^{-1})			FWHM (cm^{-1})			A (cm molecules^{-1})		
Matrix	Pure	H_2O	CO	Pure	H_2O	CO	Pure[b]	H_2O	CO
ν_9: Bending CH$_3$ rock	817	817	829	8	17	11	-	1.7×10^{-18}	2.8×10^{-18}
ν_6: Sym. CH$_3$ deformation	1369	1373	1374	5	5	4	-	6.0×10^{-19}	7.4×10^{-19}
ν_8: Asym. CH$_3$ deformation	1461	1465	1465	19	10	7	-	4.6×10^{-18}	4.1×10^{-18}
$\nu_2 + \nu_6$: Sym. CH$_3$ deformation	2736	2742	2743	4	9	6	-	2.0×10^{-19}	3.5×10^{-19}
$\nu_8 + \nu_{11}$: Asym. CH$_3$ deformation	2880	2884	2887	6	10	6	⌉	5.9×10^{-18}	6.5×10^{-18}
ν_1: Sym. CH stretching	2912	2918	2919	14	14	10	8.3×10^{-18}	9.4×10^{-19}	1.7×10^{-18}
ν_5: Sym. CH stretching	2942	2944	2947	9	11	6	⌋	2.7×10^{-18}	4.3×10^{-18}
ν_{10}: Asym. CH stretching	2957	2961	2962	6	7	8	-	9.3×10^{-20}	2.6×10^{-19}
ν_7: Asym. CH stretching	2972	2977	2981	8	13	10	1.6×10^{-17}	1.4×10^{-17}	2.2×10^{-17}

[a] Comeford & Gould (1960), Herzberg (1945)
[b] Dows (1966)

Table 2. Infrared features of C_2H_2. Entries correspond to 10 K ices: pure C_2H_2; C_2H_2 / H_2O = 1/5 and C_2H_2 / CO = 1/20

| Mode[a]	Position: ν (cm^{-1})			FWHM (cm^{-1})			A (cm molecules^{-1})		
Matrix	Pure	H_2O	CO	Pure	H_2O	CO	Pure[b]	H_2O	CO
⌈	747	-	757	⌉	-	⌉	⌉	-	⌉
ν_5	758	-	766	37	-	25	1.8×10^{-17}	-	4.0×10^{-17}
⌊	770	-	796	⌋	-	⌋	⌋	-	⌋
⌈	1370	1375	1373	⌉	⌉	⌉	⌉	⌉	⌉
$\nu_4 + \nu_5$	1391	-	1378	31	110	21	8.5×10^{-18}	3.6×10^{-18}	7.3×10^{-18}
⌊	1416	1420	1387	⌋	⌋	⌋	⌋	⌋	⌋
⌈ ν_3: CH	3227	3209	3210	⌉	⌉	16	⌉	⌉	⌉
stretching mode	3234	-	3249	11	87	⌉	6.5×10^{-17}	2.4×10^{-17}	4.2×10^{-17}
⌊	3243	3241	3257	⌋	⌋	20	⌋	⌋	⌋
$\nu_2 + \nu_4 + \nu_5$	3328	-	3323	-	-	-	-	-	-
$\nu_3 + \nu_4$	3863	3855	3881	20	-	-	-	-	-
$\nu_1 + \nu_5$	4076	4085	4088	25	45	-	-	-	-

[a] Bottger & Eggers (1964), Dows (1966)
[b] Dows (1966)

the pure ice bands are shifted to the red. This can be explained by an attractive interaction between the C_2H_6 molecules in the solid. A similar behaviour is observed for methane (Boogert et al. 1996). This redshift decreases for ethane diluted in H_2O and even more when diluted in CO, similar to what is observed for methane.
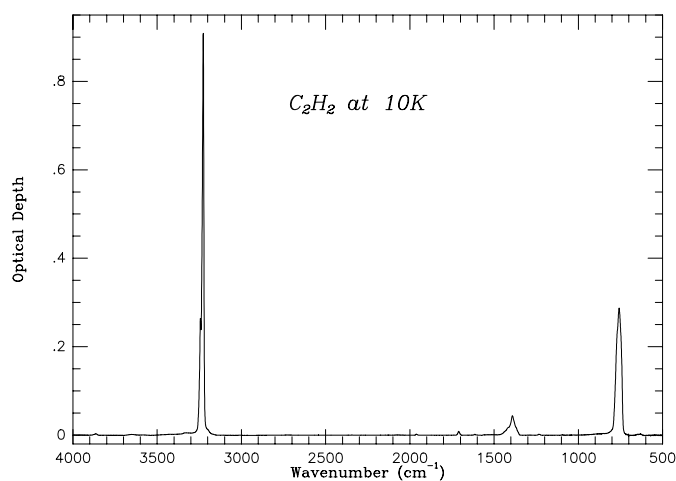
3.2. Acetylene: C_2H_2

Fig. 3 displays the IR spectrum of the pure acetylene ice. Band positions with assignment, FWHM and integrated band strength are given in Table 2. The strongest features are those of the ν_3

CH stretching mode but compared to the CH stretching modes of ethane, the ν_3 mode is shifted to the blue and overlaps with the OH stretching mode of water. When acetylene is diluted in water (C_2H_2 / H_2O = 1/5), the features become broadened and their peak strengths are severely reduced, ν_5 becoming fully blended with the libration mode of H_2O. At even higher dilutions (20/1), only the weak $\nu_4 + \nu_5$ mode can still be distinguished, all other bands being blended with water features. All acetylene features are split, probably due to the presence of distinct C_2H_2 sites in the matrix. The shift of the ν_3 and ν_5 features in the three kinds of ices is shown in Fig. 4.
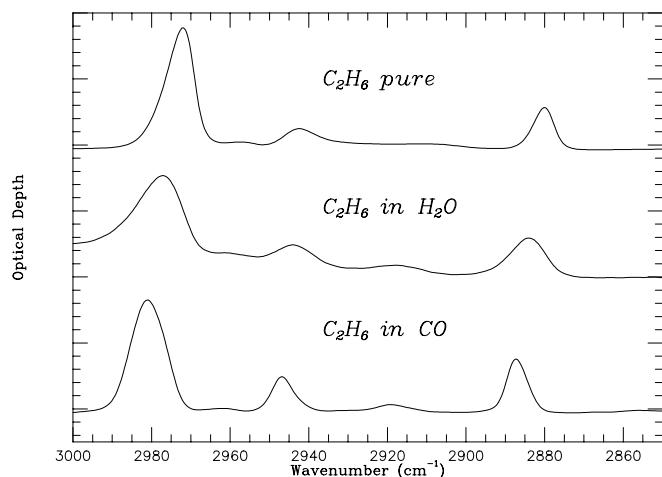
Fig. 2. Bands of C_2H_6 at 10K, for different matrices: pure C_2H_6; C_2H_6 / H_2O = 1/20 and C_2H_6 / CO = 1/20

Fig. 3. IR spectrum of pure C_2H_2 at 10K

Fig. 4. Bands of C_2H_2 at 10K, for different matrices: pure C_2H_2, C_2H_2 / H_2O = 1/5 and C_2H_2 / CO = 1/20. The dashed lines correspond to the spectrum of pure H_2O ice, indicating the blending of the C_2H_2 bands with features of the H_2O matrix
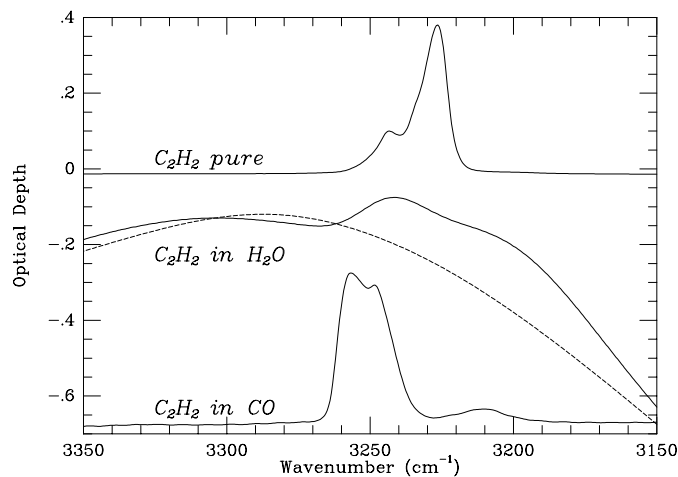
3.3. Ethanol: CH_3CH_2OH

Fig. 5 displays the IR spectrum of pure ethanol ice. The shift of the $\nu_a(CH_3)$ feature in three ice matrices is shown in Fig. 6.

Band positions with assignment, FWHM and integrated band strengths are listed in Table 3. Some features are split in different bands when ethanol is diluted in CO-rich ice, presumably due to partial break up of the hydrogen-bonding network.

3.4. Hydrogen peroxide: H_2O_2

Fig. 7 displays the IR spectrum of the purified hydrogen peroxide ice (H_2O_2/H_2O = 4/1). The $\nu_2+\nu_6$/ $2\nu_6$ feature in three ice matrices is shown in Fig. 8.

Band positions with assignment, FWHM and integrated strength are listed in Table 4. The strongest features, a combination of ν_A and ν_4 at 685 cm^{-1} and a combination of ν_5 and ν_1 at 3250 cm^{-1} are not shown because of blending with H_2O modes. The next strongest mode is the $\nu_2+\nu_6/2\nu_6$ OH bending

feature. A split of the ν_6 OH bending feature in the CO matrix is observed for this molecule as well.

3.5. Hydrazine: N_2H_4

Fig. 9 displays the IR spectrum of purified hydrazine ice (N_2H_4 / H_2O = 1/3). Band positions with assignment, FWHM and integrated band strength are given in Table 5. The strongest feature is the ν_{12} NH_2 rocking mode. A split of this feature is observed due to the breaking of some of the hydrogen bonds in the CO matrix. Two features, ν_3 at 1603 cm^{-1} and ν_{10} at 1655 cm^{-1}, cannot be seen in the spectra because of the blend with the water OH-bending mode.

3.6. Hydrozonium ion: $N_2H_5^+$

The hydrozonium ion $N_2H_5^+$ was obtained from the ice sample H_2O / N_2H_4 / HCOOH = 100/3/2. Acid-base reactions between HCOOH and N_2H_4 take place during deposition and warm-up. This is evidenced by the presence of features near 1575,

Table 3. Infrared features of CH_3CH_2OH. Entries correspond to 10 K ices: pure CH_3CH_2OH; CH_3CH_2OH / H_2O = 1/20 and CH_3CH_2OH / CO = 1/20

Mode[a]	Position: ν (cm^{-1})			FWHM (cm^{-1})			A (cm molecules^{-1})		
Matrix	Pure	H$_2$O	CO	Pure	H$_2$O	CO	Pure[b]	H$_2$O	CO
γ(OH)	674	-	641	214	-	65	-	-	5.1×10^{-18}
ρ(CH$_2$)	804	-	812	17	-	8	-	-	5.0×10^{-19}
ν(CC)	879	877	884	18	13	10	2.0×10^{-18}	3.2×10^{-18}	2.1×10^{-18}
$\lceil\nu$(CO)	1049	1045	1036	19	14	13	-	1.1×10^{-17}	1.3×10^{-18}
$\vert$	-	-	1053	-	-	21 $\rceil$	-	-	$6.7\times10^{-18}\rceil$
$\vert$	-	-	1059	-	-	$\rfloor$	-	-	$\rfloor$
$\lfloor$	-	-	1065	-	-	4	-	-	4.4×10^{-18}
ρ(CH$_3$)	1089	1091	1090	24	13	25	-	4.3×10^{-18}	4.3×10^{-18}
ρ'(CH$_3$)	1156	1163	1157	27	11	20	-	1.7×10^{-19}	1.2×10^{-19}
$\lceil\, t$(CH$_2$)	1275	1278	1262	17	15	8	-	7.0×10^{-19}	1.6×10^{-18}
$\lfloor$	-	-	1274	-	-	16	-	-	5.1×10^{-19}
$\lceil$	-	-	1318	-	-	$\rceil$	-	-	$\rceil$
$\lfloor\delta$(OH)	1329	1339	1338	49	33	40 $\rfloor$	-	3.9×10^{-18}	$1.8\times10^{-18}\rfloor$
$\lceil$	-	-	1372	-	-	7	-	-	6.3×10^{-19}
$\vert\delta_s$(CH$_3$)	1381	1386	1380	20	16	-	-	2.4×10^{-18}	4.3×10^{-19}
$\lfloor$	-	-	1396	-	-	5	-	-	1.7×10^{-18}
ω(CH$_2$)	1424	1435	1418	36	44	23	-	4.0×10^{-18}	1.6×10^{-18}
δ_a(CH$_3$)	1454	1457	1452	48	23	16	-	$4.1\times10^{-18}\rceil$	1.9×10^{-18}
δ'_a(CH$_3$)	1477	1481	-	-	19	-	-	$\rfloor$	-
δ_s(CH$_2$)	1487	-	1486	25	-	16	-	-	3.0×10^{-19}
ν_s(CH$_2$)	2884	2871	2886	73	-	45	-	-	1.1×10^{-17}
ν_s(CH$_3$), ν_a(CH$_2$)	2930	2904	2937	47	-	39	-	-	4.6×10^{-18}
ν_a(CH$_3$)	2971	2978	2982	21	18	16	-	5.6×10^{-18}	1.3×10^{-17}
$\lceil\nu$(OH)	3291	-	3283	285	-	247 $\rceil$	-	-	$5.6\times10^{-17}\rceil$
$\vert$	-	-	3379	-	-	$\vert$	-	-	$\vert$
$\vert$	-	-	3408	-	-	$\vert$	-	-	$\vert$
$\lfloor$	-	-	3448	-	-	$\rfloor$	-	-	$\rfloor$

[a] Mikawa et al. (1971)
[b] Carlon (1972)
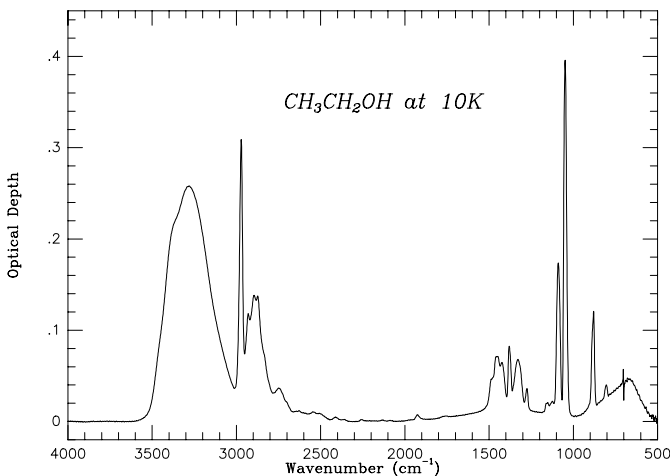
Fig. 5. IR spectrum of pure CH_3CH_2OH at 10K

1382, and 1355 cm^{-1} which can be ascribed to HCOO$^-$ (Ito & Bernstein 1956). During warm-up to 120 K these bands grow by about a factor of four, with a simultaneous strong decrease of the N_2H_4 bands and the disappearance of the HCOOH bands. Acid-base reactions are known to proceed efficiently at cryogenic temperatures in a large number of cases (Ritzhaupt & Devlin 1977; Zundel & Fritsch 1984).

To sort out the IR spectrum containing features of H_2O, N_2H_4, HCOOH, HCOO$^-$ and $N_2H_5^+$ we compared it to a number of mixtures. These were HCOOH diluted in water, NH_3 diluted in water and N_2H_4 diluted in water. Moreover, we compared with H_2O / HCOOH / NH_3 = 100/5/20 and HCOOH / NH_3 = 1/1 after warm-up to 80 K. The acid–base reactions which take place in these mixtures produce HCOO$^-$ and NH_4^+ (Ito & Bernstein 1956; Ritzhaupt & Devlin 1977; Schutte et al. 1998, in preparation). This comparison therefore distinguishes the features of HCOO$^-$. Three residual features in the spectrum of the H_2O / N_2H_4 / HCOOH = 100/3/2 sample could not be identified and were assigned to $N_2H_5^+$ (Table 6). These band grow during warm-up at the same rate as the HCOO$^-$ features, supporting the assignment with the counter-ion.

Table 4. Infrared features of H_2O_2. Entries correspond to 10 K ices: H_2O_2 / H_2O = 4/1 ($H_2O_{mix.a}$); H_2O_2 / H_2O = 1/17 ($H_2O_{mix.b}$) and H_2O_2 / H_2O / CO = 10/3/90

Mode[a]	Position: ν (cm^{-1})			FWHM (cm^{-1})			A (cm molecules^{-1})		
Matrix	$H_2O_{mix.a}$	$H_2O_{mix.b}$	CO	$H_2O_{mix.a}$	$H_2O_{mix.b}$	CO	$H_2O_{mix.a}$	$H_2O_{mix.b}$	CO[b]
ν_3: torsion, libration	889	-	-	25	-	-	-	-	-
ν_6: OH bending	1389	1411	1325	148	-	41	7.0×10^{-18}	-	9.6×10^{-18}
	-	-	1439	-	-	146	-	-	
$\nu_2 + \nu_6$, $2\nu_6$: OH bending	2837	2853	2865	100	80	111	1.5×10^{-17}	1.8×10^{-17}	5.0×10^{-18}

[a] Giguère & Harvey (1959), Miller & Hornig (1961)
[b] Valero et al. 1981

Table 5. Infrared features of N_2H_4. Entries correspond to 10 K ices: N_2H_4 / H_2O = 1/3 ($H_2O_{mix.a}$); N_2H_4 / H_2O = 1/13 ($H_2O_{mix.b}$) and N_2H_4 / H_2O / CO = 1/3/90.

Mode[a]	Position: ν (cm^{-1})			FWHM (cm^{-1})			A (cm molecules^{-1})		
Matrix	$H_2O_{mix.a}$	$H_2O_{mix.b}$	CO	$H_2O_{mix.a}$	$H_2O_{mix.b}$	CO	$H_2O^b_{mix.a}$	$H_2O_{mix.b}$	CO
ν_6: NH$_2$ rock.	905	-	870	-	-	76	-	-	-
	-	-	996	-	-	12	-	-	
	-	-	1031	-	-		-	-	
	-	-	1053	-	-	62	-	-	
	-	-	1065	-	-		-	-	
ν_{12}: NH$_2$ rock.	1093	1099	1094	90	79	28	1.9×10^{-17}	2.2×10^{-17}	2.7×10^{-17}
ν_4: NH$_2$ wagg.	1292	1290	1283	56	62	30	3.2×10^{-18}	4.8×10^{-18}	3.4×10^{-18}
ν_{11}: NH$_2$ wagg.	1345	1348	1335	69	65	58			
ν_2: NH$_2$ sym. stretching	3211	3216	3215	60	51	46	-	-	-
ν_1, ν_8: NH$_2$ antis. stretch.	3350	3353	3357	38	39	56	-	-	-

[a] Roux & Wood (1983), Durig et al. (1966)
[b] Roux & Wood (1983)

Table 6. Infrared features of $N_2H_5^+$ obtained by deposition of H_2O / N_2H_4 / HCOOH = 100/3/2 at 10 K.

| Position: ν (cm^{-1})	FWHM (cm^{-1})	A (cm molecules^{-1})
981	21	4.3×10^{-18}
1136	43	5.4×10^{-18}
2096	56	2.7×10^{-18}

4. Comparison to observations

The spectra of the species of this study are compared to spectroscopy of the obscured infrared source NGC 7538:IRS 9. This heavily obscured object has been especially well studied over the entire mid-IR range both from the ground and by the Infrared Space Observatory (Allamandola et al. 1992, Schutte et al. 1996b, Whittet et al. 1996). NGC 7538:IRS 9 is thought to be a massive protostellar object with an associated infrared reflection nebula deeply embedded in a dense molecular cloud (Werner et al. 1979). Its infrared spectrum shows deep ice absorption bands (Whittet et al. 1996)

While the obscured source W33A has a larger ice column density than NGC 7538:IRS 9 which, in principle, would make it more sensitive for probing trace constituents, the large depth of the 3 μm H_2O feature and its associated long-wavelength shoulder decreases the flux level in the region where the strongest bands of ethane and ethanol are located. This results in a low S/N in this spectral regio (Allamandola et al. 1992). Once more sensitive instruments will become available, this source should enable a very deep search for these molecules. Other sources have either considerably smaller ice column densities then NGC7538:IRS9 or have less complete spectral coverage.

The most stringent upper limits for ethane, ethanol, and hydrogen peroxide are obtained from the region 3000 – 2700 cm^{-1}. Ethane and ethanol have sharp and intense CH stretching modes in this region, while for H_2O_2 the strongest feature which is not severely blended with H_2O bands or the interstellar 6.8 μm
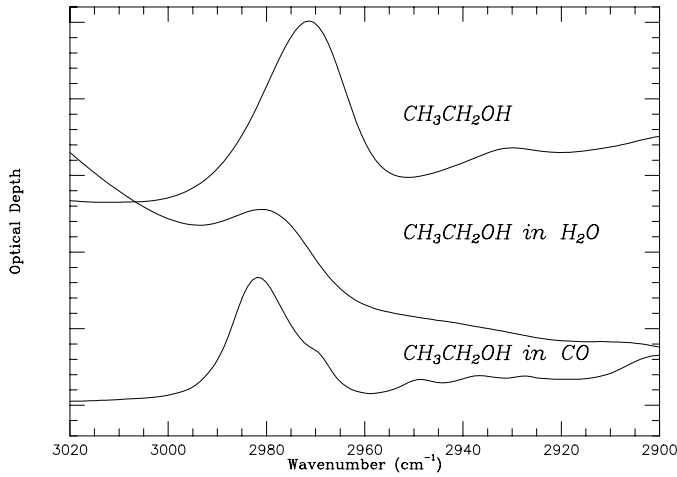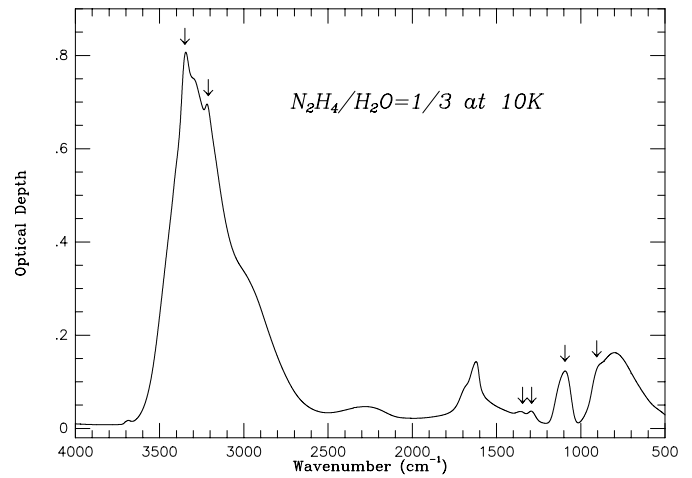
Fig. 6. Bands of CH_3CH_2OH at 10K, for different matrices: pure CH_3CH_2OH; CH_3CH_2OH / H_2O = 1/20 and CH_3CH_2OH / CO = 1/20
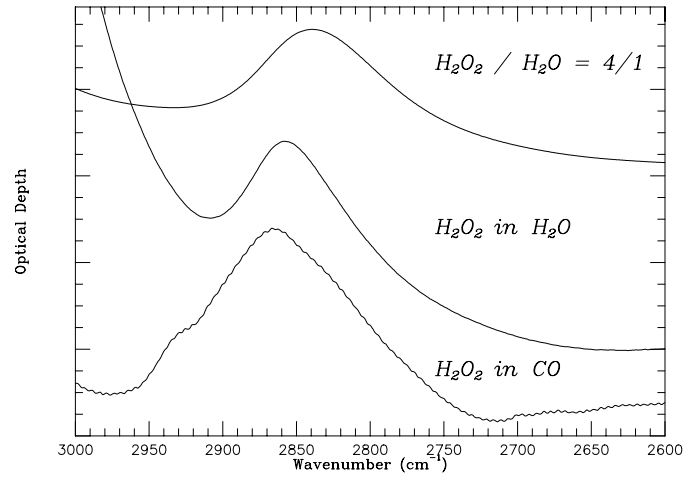
Fig. 8. Bands of H_2O_2 at 10K, for different matrices: H_2O_2 / H_2O = 4/1; H_2O_2 / H_2O = 1/17 and H_2O_2 / H_2O/ CO = 10/3/90
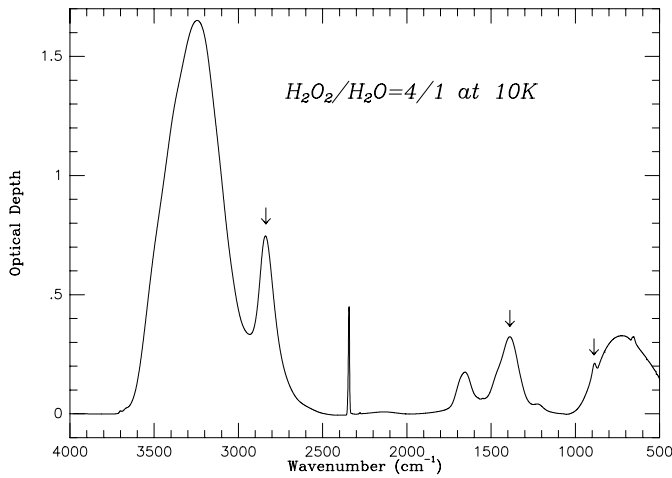
Fig. 7. IR spectrum of H_2O_2 / H_2O = 4/1 at 10K. Arrows indicate features which are exclusively due to H_2O_2

Fig. 9. IR spectrum of N_2H_4 / H_2O = 1/3 at 10K. Arrows indicate features of N_2H_4.

absorption feature (Schutte et al. 1996b) is the broad $\nu_2+\nu_6/2\nu_6$ mode at 2850 cm^{-1}. While ethanol has also a strong CO stretching mode near 1040 cm^{-1}, this feature would be blended with the corresponding band of CH_3OH and is therefore not suitable to obtain an upper limit.

Medium- ($\nu/\Delta\nu$ = 800) and low resolution spectroscopy ($\nu/\Delta\nu$ = 180) between 3000–2700 cm^{-1} for the protostar NGC 7538:IRS 9 was reported by Allamandola et al. (1992). Fig. 10 shows the range of the spectrum which contains the CH stretching modes of ethanol and ethane. The optical depth scale was obtained by substracting a linear baseline from the original spectrum (Allamandola et al. 1992). The strong C-H stretching modes of ethane and ethanol near 2975 cm^{-1} are not distinguishable. The OH bending mode of H_2O_2 was searched for unsuccessfully in the low resolution spectrum.

Table 7 presents the calculated upper-limits. They are derived by estimating the maximum peak depth τ_{max} of the fea-

ture that may still be consistent with the observed absence of the band. The column density upper-limit is then obtained from:

$$N < \frac{\tau_{max}.FWHM}{A} \tag{3}$$

where $FWHM$ and intrinsic band strength A have been experimentally derived. The column density of water ice towards NGC 7538:IRS 9 is 8.0×10^{18} molec. cm^{-2} (Schutte et al. 1996b). Thus, one can express the upper-limit as a percentage of the water ice abundance. Upper limits are given both for the CO and H_2O dominated ice matrices.

For acetylene a rather strict upper limit can be obtained from the sharp ν_3 band of C_2H_2 diluted in CO near 3250 cm^{-1}. This feature would be superimposed on the strong 3300 cm^{-1} (3 μm) band of H_2O. While for NGC 7538:IRS9 spectroscopy in this region is difficult due to the great depth of the H_2O band, the general absence of this feature towards embeddded objects (e.g., Smith et al. 1989) sets an upper limit of 1.4% for C_2H_2 diluted in CO. Due to strong broadening, the upper limit derived
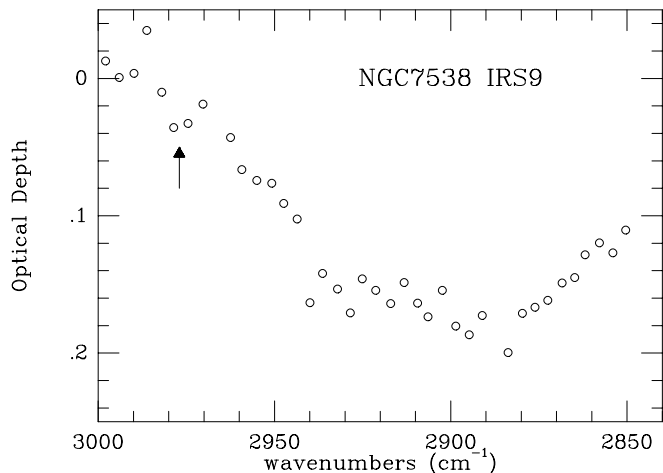
Fig. 10. IR spectrum of NGC 7538:IRS 9 (from Allamandola et al. 1992). The arrow indicates the position of the main CH stretching mode of ethane as well as ethanol.

Table 7. Upper-limits for the column density and the abundance relative to H_2O ice of solid ethane, ethanol and hydrogen peroxide towards NGC7538:IRS9

Molecules	position (cm^{-1})		Column density (cm^{-2})		Upper-limit (%)	
Matrix	H_2O	CO	H_2O	CO	H_2O	CO
C_2H_2	3241	3257	–	–	10^a	1.4^a
C_2H_6	2977	2981	2.9×10^{16}	1.5×10^{16}	0.4	0.2
CH_3CH_2OH	2978	2982	9.8×10^{16}	3.0×10^{16}	1.2	0.4
H_2O_2	2853	2865	4.9×10^{17}	1.5×10^{18}	5.2	18.7

^{a} General upper limits for obscured sources; see text

from the ν_3 band of C_2H_2 diluted in H_2O is much less stringent, i.e., about 10 % of H_2O.

For hydrazine and the hydrozonium ion all features are weak or severely blended with strong interstellar features (H_2O, silicates) and no significant upper-limits could be obtained. The most stringent upper limits for hydrazine were derived from the general absence of its N-H stretching modes superimposed on the H_2O 3 μm feature in obscured sources (e.g., Smith et al. 1989). These upper limits are of the order of 10 % of H_2O both for CO and H_2O dominated matrices, well above any theoretical prediction (Sect. 1).

Additional upper limits for ethane and ethanol can be derived from the Infrared Space Observatory - Short Wavelength Spectrometer (ISO-SWS) between 7 – 8 μm (1440 – 1250 cm^{-1}), using the respective deformation modes at 1385 and 1372 cm^{-1} (7.22 and 7.29 μm). However, due to the rather small intrinsic strength of the these modes, these upper limits are less stringent than the ones listed in Table 13. Even for the embedded source W33A which has a three times larger ice column density than NGC7538:IRS9 ($\sim 2.7 \times 10^{19}$ H_2O cm^{-2}, as derived from the 6 μm features, Whittet & Boogert, private communication), the upper limits are considerably less stringent than those listed in Table 13, i.e., only $\lesssim$ 4% for both ethane and ethanol.

5. Astrophysical implications

The most significant upper-limits are those for the H_2O-dominated ice since ethane, ethanol and hydrogen peroxide are assumed to be primarily produced in environments which contain significant abundances of atomic hydrogen. In such regions, formation of H_2O ice should be efficient (Tielens & Hagen 1982). Furthermore, the smaller homologues of ethane and ethanol, i.e., methane and methanol are found in water-rich ice (Boogert et al. 1996, 1997, Skinner et al. 1992, Allamandola et al. 1992).

The upper-limit to the column density of ethane divided by the column density of methane (1.3×10^{17} cm^{-2}; Boogert et al. 1996) gives a ratio ethane/methane < 0.22. This is considerably less than the ratio of 0.57 for Comet Hyakutake (Mumma et al. 1996). Of course, care should be exercised in drawing detailed conclusions from the comparison of one protostellar region and one comet, especially because the chemical evolution of high- and low-mass protostellar regions may be different (Shalabiea & Greenberg 1995). Future observations of additional comets and improved spectroscopy of high- and low-mass protostellar sources is necessary to see whether there is a persistant difference in this ratio. Nevertheless, at face value the apparent high abundance of a rather complex molecule like ethane in the comets seems to suggest that the formation of the cometary ice material could have involved some unique chemical processes. If this is the case, the difference between comet and protostellar methane to ethane ratio may derive from various basic mechanisms. With an increase of temperature, larger radicals are allowed to move on the grain surface, leading to the production of more complex molecules. Furthermore, UV photolysis can enhance the production of ethane and destroy methane (Stief et al. 1965, Gerakines et al. 1996). Also, the atomic C over atomic H ratio in the gas-phase will determine the size of the products made by grain surface chemistry, where longer carbon chains may be formed if the relative quantity of atomic C gets higher. Now, the origin of the difference in the ethane/methane ratio in Comet Hyakutake and in NGC 7538:IRS 9 can be sought in different directions. First, it could relate to the different conditions in the region where comet formation is supposed to have taken place, i.e., between the orbits of Uranus and Neptune (Mumma et al. 1993), as opposed to the region probed towards NGC 7538:IRS 9, which involves a large contribution by the cold, most outer parts of the protostellar region as well as by the molecular cloud itself. In this vision, the ethane was produced locally by processes typical for the region where planet formation took place. This could for example be the photoprocessing of the ices, e.g., by UV radiation originating from the hot accretion disk (Spaans et al. 1995). A strong UV radiation field might also enhance the quantity of atomic material in the gas-phase, stimulating the production of species like ethane on the grain surfaces, especially if warm-up of the grains enhances the mobility of radicals like CH_2 and CH_3 (Charnley et al. 1995). An alternative point of view is that the ethane formed in the molecular cloud before protostellar core formation. This could, for example, derive from a translucent cloud phase with high

atomic C abundance (e.g., Hasegawa et al. 1992, Hasegawa & Herbst 1993). In this view, the protostellar region of the sun and that of NGC 7538:IRS 9 sampled different kinds of dense cloud material. Finally, one cannot fully exclude the possibility that the somewhat elevated temperature in the comet formation region could have lead to partial sublimation of the methane and thus an enhancement of the ethane/methane ratio. This possibility needs further investigation by laboratory simulation experiments.

Which of these visions is correct could be investigated by further observations. If the ethane formed in the original molecular cloud, ethane/methane ratio like that of Comet Hyakutake should be found at least towards some protostellar objects. If the ethane production took place locally in the region of comet formation, it is expected that comets may show further anomalies in their composition, i.e., enhanced abundance of species with more than one C atom, such as ethanol.

The upper-limit of ethanol of 1.2% of H_2O is in the lower part of the abundance range predicted by Charnley et al. (1995), but may nevertheless still be sufficient to explain the gas-phase ethanol abundances in hot core regions. The low ethanol/methanol ratio towards NGC 7538:IRS 9 of ≤ 0.2 (the solid methanol abundance equals 7 % of H_2O; Allamandola et al. 1992) may indicate that methanol formed by hydrogenation of CO is dominant, but could also be still consistent with grain surface chemistry of carbon, oxygen and hydrogen atoms. Nevertheless, it is clear that, analogous to methane/ethane, grain surface chemistry is considerably more efficient in producing methanol than its more complex homologue ethanol.

The 5.2% upper limit for hydrogen peroxide towards NGC 7538:IRS 9 is consistent with all published models of dense cloud chemistry. It is in any case clear that solid H_2O_2 can only contain a small fraction of the oxygen in dense molecular clouds.

6. Conclusion

Comparison of the laboratory spectra with ground based and ISO observations of the embedded protostellar source NGC 7538:IRS 9 shows that the ice mantles in the line-of-sight contain less than 0.4 % ethane and less than 1.2 % ethanol relative to H_2O ice. Relative to their simple homologues, this gives C_2H_6 / $CH_4 < 0.25$, and CH_3CH_2OH / $CH_3OH < 0.2$. These results indicate that grain surface reactions in interstellar dense clouds favor the production of simple molecules over their more complex homologues.

Appendix A: behaviour during warm-up

Tables 8 to 13 list the behaviour during warm-up of the main infrared bands of ethane, ethanol and hydrogen peroxide as a function of temperature, both for CO and H_2O matrices.

Table 8. Characteristics of the main infrared features of C_2H_6 as a function of temperature for C_2H_6 / H_2O = 1/20

Mode[a]	Position: ν (cm^{-1})			FWHM (cm^{-1})		
Temperature (K)	10	80	120	10	80	120
ν_6: Sym. CH$_3$ deformation	1373	1373	1373	6	5	5
ν_8: Asym. CH$_3$ deformation	1465	1465	1465	10	9	8
$\nu_8 + \nu_{11}$: Asym. CH$_3$ deformation	2884	2885	2887	10	10	10
ν_7: Asym. CH stretching	2977	2980	2982	13	15	16

[a] Comeford & Gould (1960), Herzberg (1945)

Table 9. Characteristics of the main infrared features of C_2H_6 as a function of temperature for C_2H_6 / CO = 1/20

Mode[a]	Position: ν (cm^{-1})		FWHM (cm^{-1})	
Temperature (K)	10	30	10	30
ν_6: Sym. CH$_3$ deformation	1374	1374	4	4
ν_8: Asym. CH$_3$ deformation	1465	1465	7	7
$\nu_8 + \nu_{11}$: Asym. CH$_3$ deformation	2887	2887	6	6
ν_7: Asym. CH stretching	2981	2981	10	10

[a] Comeford & Gould (1960), Herzberg (1945)

Table 10. Characteristics of the main infrared features of CH_3CH_2OH as a function of temperature for CH_3CH_2OH / H_2O = 1/20

Mode[a]	Position: ν (cm^{-1})			FWHM (cm^{-1})		
Temp. (K)	10	80	120	10	80	120
ν(CO)	1045	1044	1044	14	14	14
ρ(CH$_3$)	1091	1091	1091	13	13	13
ν_a(CH$_3$)	2978	2980	2979	18	18	18

[a] Mikawa et al. (1971)

Table 11. Characteristics of the main infrared features of CH_3CH_2OH as a function of temperature for CH_3CH_2OH / CO = 1/20

Mode[a]	Position: ν (cm^{-1})		FWHM (cm^{-1})	
Temperature (K)	10	30	10	30
⌈ν(CO)	1036		13	
	1053	1053	21 ⌉	22
	1059		⌋	
⌊	1065	1065	4	3
ρ(CH$_3$)	1090	1094	25	22
ν_a(CH$_3$)	2982	2982	16	15

[a] Mikawa et al. (1971)

Table 12. Characteristics of the main infrared features of H_2O_2 as a function of temperature for H_2O_2 / H_2O = 1/17

Mode[a]	Position: ν (cm^{-1})			FWHM (cm^{-1})		
Temperature (K)	10	80	120	10	80	120
ν_6: OH bending	1411	1427	1431			
$\nu_2 + \nu_6$, $2\nu_6$: OH bending	2853	2858	2858	80	80	80

[a] Giguère & Harvey (1959), Miller & Hornig (1961)

Table 13. Characteristics of the main infrared features of H_2O_2 as function of temperature for H_2O_2 / H_2O / CO = 10/3/90

Mode[a]	Position: ν (cm^{-1})		FWHM (cm^{-1})	
Temperature (K)	10	30	10	30
⌈ ν_6: OH bending	1325	1329	41	38
⌊	1439	1434	146	145
$\nu_2 + \nu_6$, $2\nu_6$: OH bending	2865	2862	111	98

[a] Giguère & Harvey (1959), Miller & Hornig (1961)

References

Allamandola L.J., Sandford S.A., Tielens A.G.G.M., Herbst T.M., 1992, ApJ 399, 134

Bockelée-Morvan D., 1997, in I.A.U. Symp. No. 178: Molecules in Astrophysics: Probes and Processes, ed. E.F. van Dishoeck (Kluwer, Dordrecht), p. 219

Boogert A.C.A., Schutte W.A., Tielens A.G.G.M., et al., 1996, A&A 315, L377

Boogert, A.C.A., Schutte W.A., Tielens A.G.G.M., et al., 1997, A&A 317, 929

Bottger G.L., Eggers Jr. D.F., 1964, J. Chem. Phys. 40, 2010

Brown P.D., Charnley S.B., Millar T.J., 1988, MNRAS 231, 409

Carlon H.R., 1972, Applied optics 11(3), 549

Carr J.S., Evans II N.J., Lacy J.H., Zhou S., 1995, ApJ 450, 667

Charnley S.B., Kress M.E., Tielens A.G.G.M., Millar T.J., 1995, ApJ 448, 232

Comeford J.J., Gould J.H., 1960, J. Molec. Spec. 5, 474

d'Hendecourt L.B., Allamandola L.J., 1986, A&AS 64, 453

d'Hendecourt L.B., Allamandola L.J. Greenberg J.M., 1985, A&A 152, 130

Dows D.A., 1966, Spectrochim. Acta 22, 1479

Durig J.R., Bush S.F., Mercer E.E., 1966, J. Chem. Phys. 44(11), 4238

Evans II N.J., Lacy J.H., Carr J.S., 1991, ApJ 383, 674

Gerakines P.A., Schutte W.A., Greenberg J.M., van Dishoeck E.F., 1995, A&A 296, 810

Gerakines P.A., Schutte W.A., Ehrenfreund P., 1996, A&A 312, 289

Giguère P.A., Harvey K.B., 1959, J. Molec. Spec. 3, 36

Greenberg J.M., 1982. in Comets, ed. L.L. Wilkening (Univ. of Arizona press, Tucson), p. 131

Grim R.J.A., Greenberg J.M., de Groot M.S., et al., 1989, A&AS 78, 161

Hasegawa T.I., Herbst E., 1993, MNRAS 261, 83

Hasegawa T.I., Herbst E., Leung C.M., 1992, ApJS 82, 167

Herbst E., Adams N.G., Smith D., 1983, ApJ 269, 329

Herzberg G., 1945, Molecular Spectra and Molecular Structure. II Infrared and Raman Spectra of Polyatomic Molecules (Van Nostrand Reinhold Company, New York)

Hiraoka K., Ohashi N., Kihare Y., et al., 1994, Chemical Physics Letters 229, 408

Ito K., Bernstein H.J., 1956, Canadian Journal of Chemistry 34, 170

Lacy, J.H. Evans II N.J., Achtermann J.M., et al., 1989, ApJ 342, L43

Mikawa Y., Brasch J.W., Jakobsen R.J., 1971, Spectrochim. Acta 27A, 529

Millar T.J., Macdonald G.H., Habing R.J., 1995, MNRAS 273, 25

Miller R.L., Hornig D.F., 1961, J. Chem. Phys. 34(1), 265

Mumma M.J., Weissman P. R., Stern S.A., 1993, in Protostars and Planets III, eds. E.H. Levy and J.I. Lunine (University of Arizona press, Tucson), p. 1177

Mumma M.J., DiSanti M.A., Russo N.D., et al., 1996, Nat 272, 1310

Prasad S.S., Tarafdar S.P., Villere K.R., Huntress Jr W.T., 1987, in Interstellar Processes, eds. D.J. Hollenbach and H.A. Thronson, Jr. (D. Reidel Publishing Company, Dordrecht), p. 631

Ritzhaupt G., Devlin J.P., 1977, Journal of Physical Chemistry 81, 521

Roux J.A., Wood B.E., 1983, J. Opt. Soc. Am. 73(9), 1181

Schutte W.A., 1996, in The cosmic dust connection, ed. J.M. Greenberg, (D. Reidel Publishing Company, Dordrecht), p. 1

Schutte W.A., Greenberg J.M., 1997, A&A lett. 317, L43

Schutte W.A., Gerakines P.A., Geballe T.R., Greenberg, J.M., van Dishoeck E.F., 1996a, A&A 309, 633

Schutte W.A., Tielens A.G.G.M., Whittet D.C.B., et al., 1996b, A&A 315, L333

Shalabiea O.M., Greenberg J.M. 1994, A&A 290, 266

Shalabiea O.M., Greenberg J.M. 1995, A&A 303, 233

Skinner C.J., Tielens, A.G.G.M., Barlow M.J., Justtanont K., 1992, ApJ 399, L79

Smith R.G., Sellgren K., Tokunaga A.T., 1989, ApJ 344, 413

Spaans M., Hogerheijde M. R, Mundy L.G., van Dishoeck E.F., 1995, ApJ 455, L167

Stief L.J., DeCarlo J., Hillman J.J., 1965, Journal Chemical Physics 43, 2490

Tielens A.G.G.M., Hagen W., 1982, A&A 114, 245

Tejada S.B., Eggers Jr., D.F., 1976, Spectrochim. Acta 32A, 1157

Valero F.P.J., Goorvitch D., Bonomo F.S., Boese R. W., 1981, Applied optics 20(23), 4097

Werner M.W., Becklin E.E., Gatley I., et al., 1979, MNRAS 188, 463

Whittet D.C.B., Schutte W.A., Tielens A.G.G.M., et al., 1996, A&A 315, L357

Zundel G., Fritsch J., 1984, J. Phys. Chem. 88, 6295